Alexander Enoch
Institute of Perception,
Action and Behaviour,
School of Informatics,
University of Edinburgh,
Edinburgh EH8 9YL, UK
e-mail: a.m.enoch@sms.ed.ac.uk

Sethu Vijayakumar
Institute of Perception,
Action and Behaviour,
School of Informatics,
University of Edinburgh,
Edinburgh EH8 9YL, UK
e-mail: sethu.vijayakumar@ed.ac.uk

Rapid Manufacture of Novel Variable Impedance Robots

Variable stiffness and variable damping can play an important role in robot movement, particularly for legged robots such as bipedal walkers. Variable impedance also introduces new control problems, since there are more degrees of freedom to control, and the resulting robot has more complex dynamics. In this paper, we introduce novel design and fabrication methodologies that are capable of producing cost effective hardware prototypes suitable for investigating the efficacy of impedance modulation. We present two variable impedance bipedal platforms produced using a combination of waterjet cutting and 3D printing, and a novel fused deposition modeling (FDM) 3D printing based method for producing hybrid plastic/metal parts. We evaluate walking trajectories at different speeds and stiffness levels. [DOI: 10.1115/1.4030388]

1 Introduction

Physical compliance can be of great use in bipedal locomotion, potentially allowing the dynamics of a particular system to be taken advantage of (e.g., Ref. [1]), storing energy from loading, adapting to uneven terrain, and absorbing shocks (e.g., Ref. [2]). Variable impedance provides us with a path to exploiting these advantages and allows us to adapt for differing gaits and speeds, different terrains (for example, adjusting based on the softness or hardness of the terrain), loading conditions, etc., while producing a robot that is capable of a wide variety of tasks apart from just walking in a predetermined way.

We have developed a framework for optimization of torque and stiffness profiles for task based actions [3]; transferred impedance control strategies from humans to robots [4]; explored optimal control strategies for a variety of tasks, including throwing with variable stiffness [5], control of variable damping for point to point movement tasks on a robot with variable impedance actuation [6], and the use of variable impedance motion on brachiation and hopping [7].

To best explore the effects of variable impedance on bipedal locomotion, we require robots which possess the capability to physically vary the impedance of their joints around a viable operational range. A great number of designs exist for achieving variable stiffness, as well as several for variable damping. We will give an overview of these and explore their suitability for use in legged robots.

We also consider the manufacturability of the actuators and present our work in designing and building complex bipedal robots which can be produced with minimal tooling and equipment. We demonstrate the utility of rapid manufacturing technologies including waterjet cutting and 3D printing.

Based on these concepts, in this paper we present BLUE (Fig. 1(*a*)), a bipedal robot with variable impedance joints, which was primarily constructed from waterjet cut aluminum, and introduce miniBLUE (Fig. 1(*b*)), a smaller variable impedance biped with more joints, manufactured using SLS 3D printing. miniBLUE is designed to allow the exploration of different types of joint, allowing the variable stiffness element to be easily swapped.

The use of selective laser sintering (SLS) 3D printing to produce structural compliant elements with a designed stiffness is shown, as well as our technique for producing hybrid FDM/waterjet cut parts (Fig. 1(*c*)). We show that these rapid manufacturing techniques can be used to enable the quick and cost effective production of complex robots, without the need for complex machining. We then present our control system for the robots, including distributed Ethernet based electronics, and show preliminary results in software and on the hardware.

Manuscript received August 1, 2014; final manuscript received April 8, 2015; published online August 18, 2015. Assoc. Editor: Aaron M. Dollar.

2 Variable Impedance for Legged Robots

Walking is a dynamic task that involves contact with the ground. Ground reaction forces must be dealt with or without over-stressing the hardware, and ideally without the loss of too much energy. If the natural dynamics of the system can be used, there is potential to greatly reduce the amount of energy used for walking. Furthermore, in any real environment, there will be potential obstacles and irregularities in the ground surface—compliance can provide the opportunity to at least partially adapt around such disturbances.

It is a fundamental design criterion that the joints of the robot are able to produce the mechanical power to produce locomotion, but in addition to this the variable stiffness joints should also be as energy efficient as possible—ideally not wasting power merely to change stiffness. In many designs, the available energy storage or maximum output torque also changes with stiffness. To produce locomotion at high stiffnesses, the robot must be capable of high output torques at high stiffness values and should provide as much energy storage (and hence compliant range) as possible at these high stiffnesses.

Our high-level criteria when selecting a mechanism for variable stiffness are therefore:

- deliver the required torque without excessive or exhaustive deflection
- produce high torque at high stiffness values
- energy efficient when changing stiffness
- energy storage independent of stiffness level
- maximized elastic deformation range
- simple to manufacture

2.1 Variable Impedance Mechanisms.

Many mechanisms have been developed for variable impedance actuation, both for stiffness and damping [8,9]. When producing a platform with variable impedance capabilities, it is necessary to review this array of potential implementations, in our case with respect to the design criteria listed above.

In general, variable stiffness actuator designs can be grouped into those which rely on an antagonistic arrangement of compliant elements, and those which have a series elastic layout. Antagonistic layouts typically change the apparent stiffness of the joint by changing the pretension of one or more elastic elements.

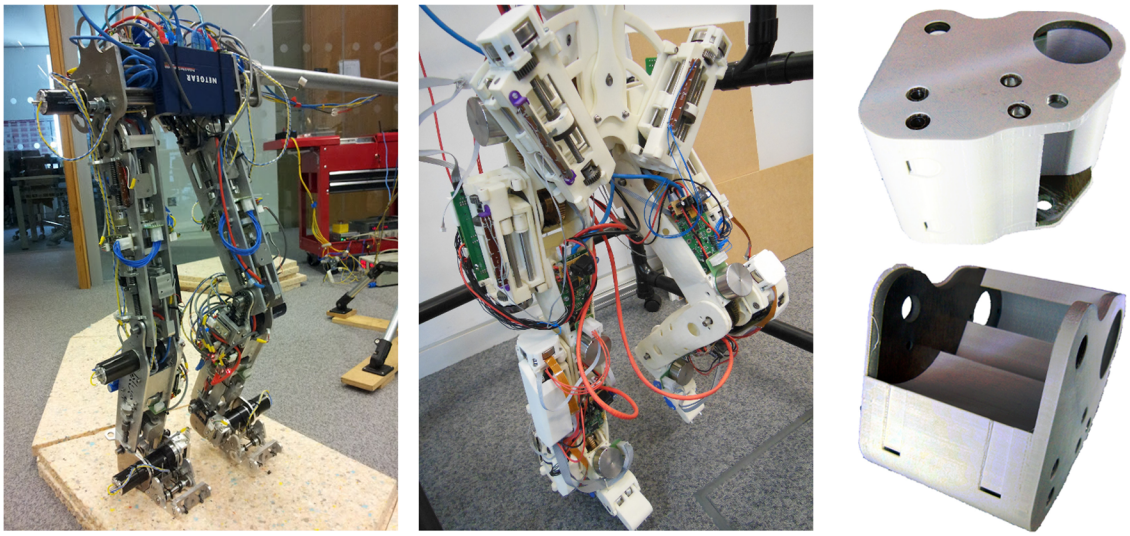

Fig. 1 BLUE and miniBLUE, robots capable of mechanically varying the dynamics of their joints, and 3D printed part with waterjet cut aluminum embedded inside during printing

Similarly, some series mechanisms are pretension based, while others actually change the stiffness of the joint by changing the geometry of the layout, without the need to load a spring.

2.2 Selecting Variable Impedance Mechanisms. Typically, variable stiffness mechanisms which are the simplest to build are pretension based. These include antagonistic-based mechanisms such as the Edinburgh-SEA [10] and series pretension mechanisms such as the MACCEPA [11].

Mechanisms which do not rely on pretension include the AWAS [12], AWAS-II [13], MIA [14,15], the magnetic mechanism of Choi et al. [16] and the CompACT [17]. The MIA and Choi mechanisms do not allow the use of all of their elastic potential at all stiffness settings. Table 1 summarizes key characteristics of various types of variable stiffness actuators.

Antagonistic mechanisms are generally more simple to manufacture. In its most basic form, a compliant antagonistic actuator consists of a joint which is pulled in one direction by an actuator through one compliant element, and in the other direction by a second actuator through a second compliant element. More complex antagonistic designs are possible, for example, as shown in Ref. [21].

Normal linear springs cannot be used in the traditional antagonistic layout, as they produce a stiffness function of $K = (dT/d\theta) = 2R^2k$, where R is the lever arm radius, and k is the spring constant of the linear springs. The stiffness is not a function of actuator contraction x_1 or x_2, and thus the stiffness is constant and not controllable, unless the individual spring constant k is variable. It is necessary to use nonlinear springs in order to produce a joint with controllable stiffness, and for this reason most antagonistic variable impedance actuator (VIA) designs concentrate on designing a nonlinear spring, or arranging linear springs in such a way as to create nonlinearity.

If the nonlinear springs used have a quadratic spring function of the form $F_s(x) = ax^2 + c$, then the resulting joint will have a stiffness of $K = 2aR^2(x_1 + x_2)$. This is a function of x_1 and x_2 and allows the stiffness to be controlled, but is independent of deflection, θ, and thus gives a linear force–deflection profile. The corresponding equilibrium position equation for these quadratic springs is $\theta_{eq} = -((x_1 - x_2)/2R)$. By changing $(x_1 + x_2)$ while keeping $(x_1 - x_2)$ constant, stiffness can be adjusted while keeping equilibrium position constant. The opposite action will vary equilibrium position with constant stiffness. Using quadratic springs, therefore, provides a relatively simple decoupling of stiffness and equilibrium position and gives a linear stiffness profile.

Most antagonistic methods rely on changing the pretension in the springs in order to vary stiffness, as described above. For a simple analysis, we can consider the mechanical energy cost of increasing the stiffness of the joint from a state with no pretension. We will consider ideal quadratic springs of function $F_s(x) = -ax^2$ and move both actuators in synchrony to keep $x_1 = x_2$, varying $(x_1 + x_2)$ while keeping $(x_1 - x_2)$ constant.

The energy consumed will be

$$E = 2\int_0^{x_s} ax^2 dx = \frac{2}{3}ax_s^3 \tag{1}$$

Using the equation for joint stiffness with quadratic springs when $x_s = x_1 = x_2, K = 4aR^2x_s$, the energy required can be expressed in terms of the resulting joint stiffness

$$E = \frac{Kx_s^2}{6R^2} \tag{2}$$

Energy usage to increase stiffness is therefore proportional to the square of actuator contraction, as well as the resulting stiffness. To extract some real numbers, it would be realistic that the final actuator contraction, x_s is equal to the lever arm radius R, and the equation then simplifies to $E = (K/6)$. If the achieved stiffness is 150 Nm/rad, then the energy used to achieve this stiffness would be 25 J. This represents a substantial amount of energy utilized merely to increase stiffness, and although it is stored in springs, it is generally not recoverable in any useful way.

For our robots, BLUE and miniBLUE, we can evaluate the characteristics of the various types of variable stiffness mechanisms against the design criteria given above.

As can be seen from Table 1, the AWAS-II or compACT VSA mechanisms are arguably the most suitable for our application. These mechanisms can produce high torques at high stiffnesses, do not require pretensing to change stiffness, provide their full elastic potential at all stiffnesses, and have an exemplary range of stiffnesses. However, these mechanisms are relatively complex to manufacture.

However, a modified version of the AWAS mechanism, which produces even compression of the springs and increases the elastic range of the joint, provides a balance between performance and manufacturability.

Table 1 Variable stiffness mechanisms. Many antagonistic designs concentrate on creating nonlinear springs which can be used in antagonistic designs. In many designs, the potential for energy storage decreases as stiffness increases. T_{max} versus k shows how the maximum torque provided by the mechanism changes as stiffness increases; in antagonistic designs, the maximum output torque decreases as stiffness increases, whereas in most other designs the opposite occurs. The energy cost of changing stiffness in antagonistic designs is typically higher than for other designs, as it involves prestressing a plurality of springs.

VSA	Type	Nominal stiffness	Energy storage versus stiffness	Max elastic deformation range	Stiffness linearity	T_{max} versus k	Complexity of manufacture	Energy cost to change stiffness
"Pull only" antagonistic	Antagonistic	Low → high	↓	360 deg+	If quadratic springs	↓	Simple	● ●
"Pull–push" antagonistic	Antagonistic	0 → high	↓	90 deg	If quadratic springs	↓	Simple	● ●
Bidirectional antagonistic	Antagonistic	low → medium	↓	360 deg+	Hardening	↓	Simple	● ●
Edinburgh SEA [10]	Antagonistic	Low	↓	90 deg	Highly nonlinear	↓	Very simple	●
MACCEPA [11]	Series pretension	Low	↓	180 deg	Highly nonlinear	↑	Simple	●
VS-joint [18]	Series pretension	0 → high	↓	14 deg	Customisable	↑	Complex	●
Uemura and Kawamura [19]	Series pretension	Low	↑	180 deg	Highly nonlinear	↑	Simple	●
AwAS [12]	Series	Low → high	—	11.5 deg	Near linear	↑	Average	—
AwAS II [13] and CompACT VSA [17]	Series	0 → ∞	—	40 deg	Near linear	↑	Complex	—
MIA [14]	Series	Low → high	↓	20 deg	Near linear	↑	Simple	—
Choi et al. [20]	Series	Medium → high	↓	11.5 deg	Near linear	↑	Complex	—

Fig. 2 Schematic of the variable stiffness transmission. The motor attached to the input link drives the intermediate arm which, through a pair of compression springs, delivers torque to the output link. A second motor adjusts the position of the compression springs, and hence the distance *r* in order to change the stiffness.

A render of the modified variable stiffness mechanism is shown in Fig. 2. A pair of wave compression springs is used to provide the physical compliance and energy storage. The stiffness is adjusted by moving these springs linearly toward or away from the axis of rotation of the joint. The torque and stiffness (derivative of torque with respect to deflection) equations for this joint are

$$T = \frac{r^2 K_s}{2}\sin(2\theta) \tag{3}$$

$$K = \frac{dT}{d\theta} = r^2 K_s \cos(2\theta) \tag{4}$$

where θ is the compliant deflection, r is the distance of the springs from the axis of rotation, and K_s is the spring constant of the springs. The characteristic curves of the joint are shown in Fig. 3, in this case for the springs used in the knees of BLUE.

When the maximum compression of the spring is reached, the transmission hits a hard stop, and effectively becomes a rigid joint. The maximum deflection required to reach this rigid limit is given by

$$\theta_{max} = \sin^{-1}\left(\frac{l_{comp}}{r}\right) \tag{5}$$

where l_{comp} is the maximum compression of the spring.

There are several ways to achieve variable damping, including altering the channel size of hydraulic dampers [22], using piezoelectric stacks [23], and magnetorheological damping [24]. One way of achieving variable damping that does not require energy to be supplied in order to perform the damping is motor braking. This involves connecting an additional motor in parallel with the joint and controlling the braking of the motor by changing the percentage of time for which the motor terminals are directly connected together [6].

The maximum achievable damping with a permanent magnet DC motor is $T_b(\dot{\theta}) = -\left(n^2\kappa_T\kappa_{\dot{q}}/R_e\right)\theta$, where $n:1$ is the gear ratio, κ_T and $\kappa_{\dot{q}}$ are the motor torque and speed constants, and R_e is the equivalent resistance of the motor. The downside to the energy efficient damping and ease of manufacture is the limited range of damping available, and the weight that the additional motor adds to the assembly.

3 Hardware Design

We have built two platforms to investigate the use of variable impedance joints in bipedal robots. To scale up toward full three-dimensional motions, we have produced a planar robot, BLUE,

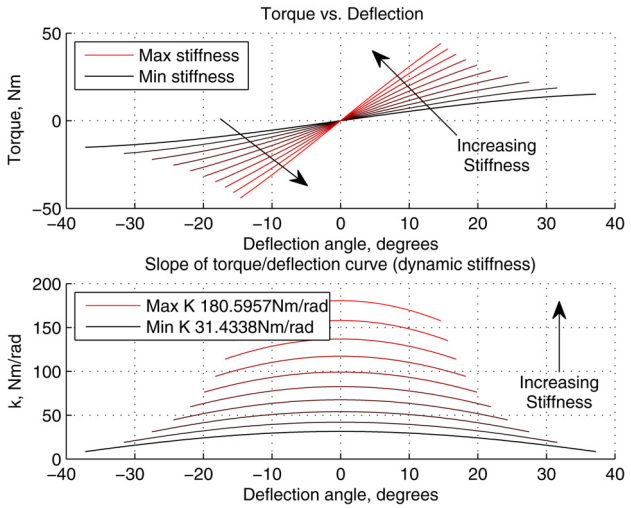

Fig. 3 Torque and stiffness curves for the variable stiffness mechanism in the knees and ankles of BLUE

and a robot with two degrees of freedom in its hips—miniBLUE. miniBLUE is also designed to be a modular platform for experimenting with different joint architectures.

3.1 BLUE: A Planar Biped Made Using Waterjet Cutting. BLUE [18] (see Figs. 1(*a*) and 4) was designed to be 3/4 the size of an adult male, with a hip rotation height of 695 mm. BLUE was designed as a planar biped, containing joints only in the sagittal plane. It has variable impedance joints in each leg, in addition to feet with compliant arches and toes. While the robot does require lateral support from a boom arm, it is free to move in the sagittal plane and reproduce walking or other locomotion in this plane. Starting with a planar robot simplifies balance and reduces the complexity of the control problem while allowing key issues with bipedal locomotion to be investigated.

We set a target weight for BLUE of around 20 kg, and knowing this and the size of the robot, we looked at studies of human walking kinetics (e.g., Ref. [25]) in order to compare likely required torques with compliant deflections and aid in the selection of springs for the joints. These values were later checked by dynamic simulation of the design. The springs can be changed in the variable stiffness joints, if it is desired to change the range of available stiffness and output torque.

The complexity of three dimensional shapes was minimized for BLUE; it was designed to essentially be a "flat-pack" robot. The main difficulty in manufacture was producing the three dimensional features required for connecting the parts together. Flanged bushings made of self-lubricating plastic (iglidur G, by Igus GmbH, Cologne, Germany) were used around the joints; these provide hard wearing bearing surfaces with a small thrust bearing surface, are compact, and are easy to locationally fix.

Aside from the waterjet cutting, size critical holes were drilled and reamed or, where appropriate, tapped. Keyways were created with a manual broach. These tasks can be performed with a simple pillar drill if necessary. The only remaining machining tasks involved turning shafts and milling three dimensional features. However, these tasks accounted for a large portion of the overall construction time.

The use of waterjet cutting for BLUE therefore allowed the general shape to be produced very quickly, but in order to tie the robot together a number of 3D parts or features were required, and machining these took time.

3.2 miniBLUE: A Robot Made Using SLS 3D Printing. BLUE is a sagittal plane biped and is thus unable to move its hips in and out. While this movement only represents a small portion of the total mechanical power used while walking, the lack of it

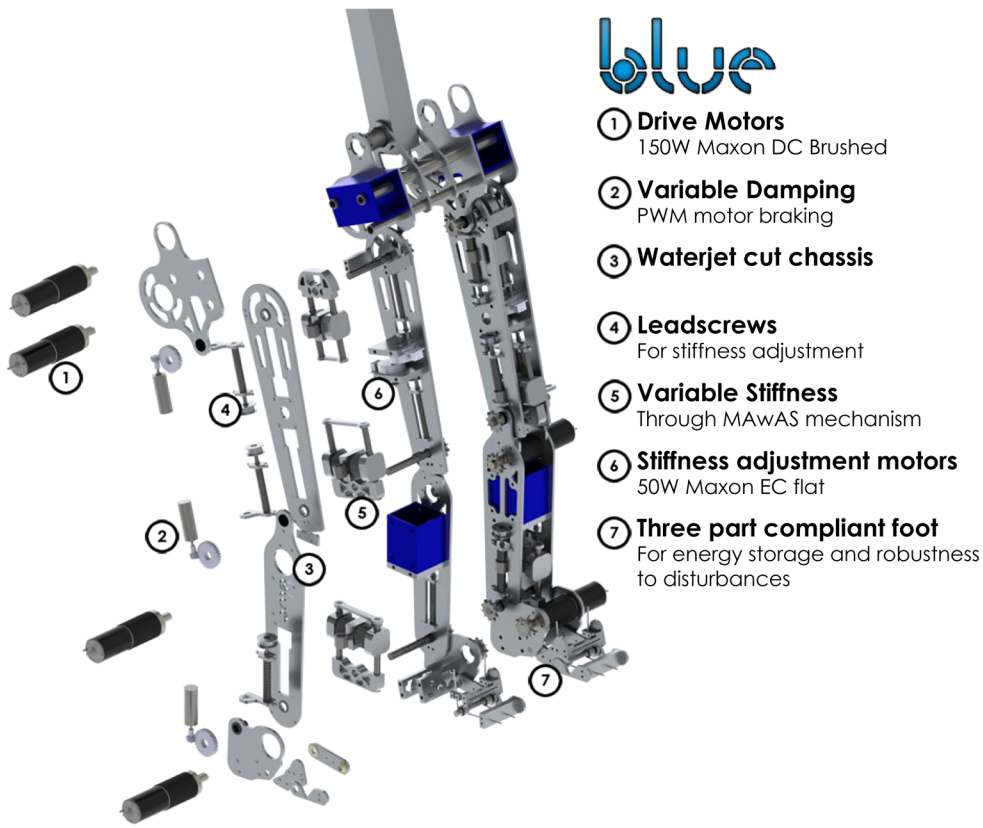

Fig. 4 BLUE: a planar biped

does cause some problems with clearance during foot swing-through.

To overcome these issues and move further toward full three dimensional walking movement, we constructed a robot capable of hip adduction and abduction—inward and outward movement of the hips.

miniBLUE was designed to be only 1/2 the height of the average adult American male, and 3D printing was the primary manufacturing technique utilized.

A key feature of the miniBLUE platform (Fig. 1(*b*)) is its highly modular joint structure. The series elastic component in each variable stiffness joint is provided in a "pod" on the side of the leg. The elastic element can be easily changed if required, for example, to try different designs of variable stiffness joint. Initially, variable stiffness joints were produced based on the same design as those used for BLUE.

The same modified-AWAS variable stiffness joints were used for miniBLUE, the only difference being they were implemented in a different way. MAWAS "pods" affix to the side of the joints and torque is transferred from the drive shafts, through these pods to the output link. A render of one of these pods is shown in Fig. 5(*b*). This figure shows that the superstructure of the pod is all 3D printed and contains holes for inserting lengths of shaft to allow the variable stiffness mechanism to move. These shafts are press-fit into the printed part. A 3D printed carrier accepts the leadscrew nut directly, and the only finishing operation required to assemble one of these pods is the turning of shoulders onto the leadscrew.

3.3 3D Printing for Compliant, Structural Parts. These pods are an integral part of the design of miniBLUE, since as well as simplifying the construction of miniBLUE, the use of these pods allows the variable stiffness units themselves to be quickly altered or replaced. This allows, for example, the springs to be replaced if a stiffer or softer joint is wanted. Additionally, if a different design of variable stiffness joint is desired, this can be fabricated and then quickly attached to the robot. The sensors which measure joint output position and compliant deflection are mounted on the main body of miniBLUE, further simplifying the pods. Alternatively, a simple plate can be attached which transforms the joint into a rigid joint (with appropriate shock absorption). We therefore have created a bipedal robotic platform which allows different series elastic mechanisms to be investigated.

Variable damping is again achieved by connecting an additional motor in parallel with the variable stiffness drive. In this case, the damping forces are relatively low and can be borne by plastic gearing. 3D printing allows us to print the link side gear directly onto the link part, reducing the size of the assembly and simplifying construction. This is shown in Fig. 5(*c*).

Companies such as Shapeways will 3D print parts for users in a variety of materials, using a variety of techniques. The material referred to as "White Soft and Flexible" is PA 2200 Nylon by EOS GmBH and has a reported tensile strength of 48 MPa. We use this material in an SLS printing process to make the 3D printed parts of miniBLUE.

Worm gearing is used on the output from the 70 W Maxon EC45 drive motors. In order to avoid loading the motor, the worm itself is sandwiched between two thrust bearings which transfer the load to the 3D printed structure. Finite element analysis (FEA) showed that the maximum stresses in the femur part occur at the point where the load from the worm is transferred to the link, however, these only reach one third of the rated ultimate tensile stress for the material.

Sintered Nylon is quite machinable and can be threaded for light loads; for more heavy duty threads we utilize threaded brass inserts with knurled outer surfaces. For highly toleranced holes, it is necessary to drill and ream the parts. The porous nature of SLS parts can also cause issues around drive components, where the plastic can be plastically compressed.

The flexible properties of materials such as PA 2200 can be used advantageously in robotic structures, for example, to introduce compliance.

Compliant materials are beneficial in the feet of legged robots, which are subject to ground contact. A human foot is composed of a great number of small bones which make it capable of moulding to the contours of the ground and flexing to absorb shocks and store energy in ways which a rigid foot could not. The toes are particularly important since they spread the weight bearing area which is available during the later stages of the stance phase of walking, before toe-off.

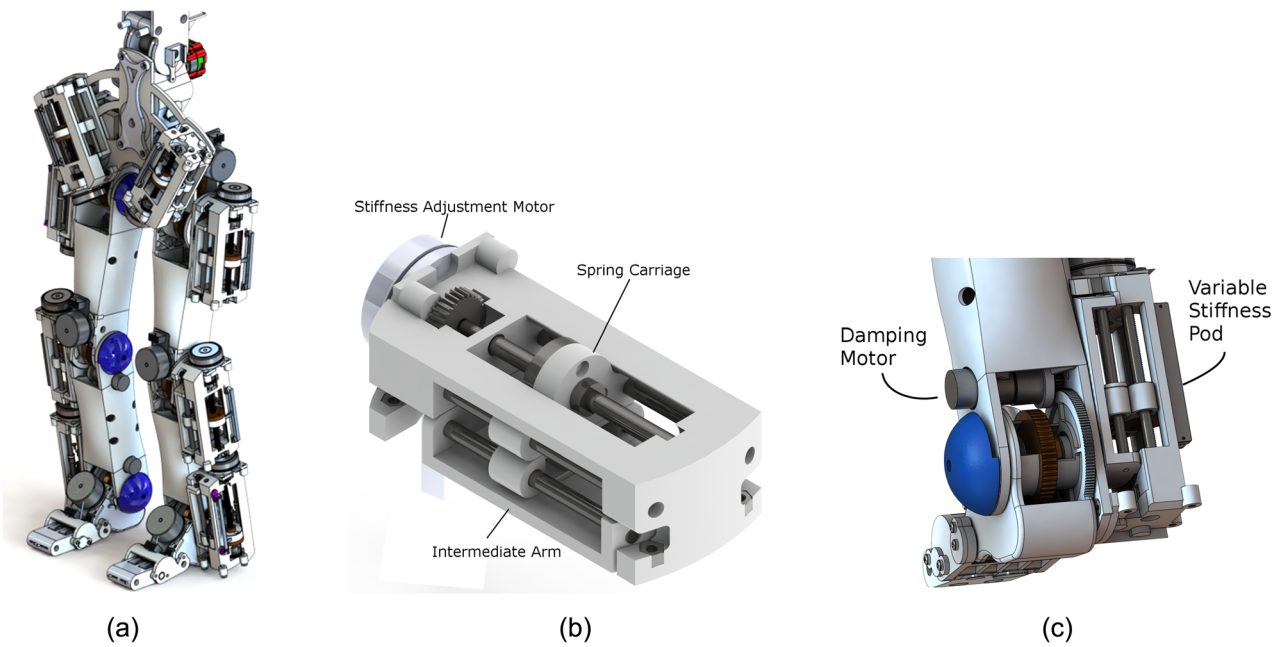

Fig. 5 (*a*) miniBLUE: a biped with 2DOF hips and torso; (*b*) a variable stiffness pod which attaches to the side of miniBLUE, forming the series elastic element in the drive. A motor on the pod drives the central leadscrew, adjusting the position of the load bearing springs and thereby changing the joint stiffness; and (*c*) miniBLUE joint architecture: damping motor connectivity in parallel with variable stiffness pod.

The longitudinal arch of the foot is an important structure for absorbing shocks and providing elasticity in the foot. Ker et al. [26] conducted experiments to determine the elasticity and energy storage capability of the spring in the arch of the human foot. They determined that the arch of the foot stores enough strain energy to make running more energy efficient. It can be observed that the arch deforms during walking [27], additionally, there is evidence that the arch of the foot is stiffer toward toe-off [28].

3.4 Compliant Foot Arches. In our robots, we create an elastic joint of high stiffness in the middle of the foot. When the elastic range is exhausted, the joint becomes rigid rather than plastically deforming or breaking.

The placing of the mid-part of the foot in miniBLUE is shown in Fig. 6(*a*). Before the elastic limit of the part is reached, a hard stop is hit and the foot becomes effectively solid. While the arch is shown as a separate part in this figure it can be fabricated as one piece along with the rear foot. In this way, the part is primarily quite rigid, but has a flexible arch with the compliant characteristics we desire, all in one piece.

Such elastic elements are designed in the feet of the robots and manufactured using 3D printing. The geometry was optimized using FEA to reach a given stiffness profile, keeping below the tensile strength of the printed material. The analysis indicates that the arch will produce a deflection of 14 deg at 2.25 Nm of loading of the hinge of the arch.

Figure 6(*c*) shows a plot of the applied load on the arch versus the maximum linear deflection, for both the simulated part from FEA analysis and from load testing on an actual fabricated part. The part was placed in a custom jig and statically loaded by the application of distributed weight to the loading surfaces. As can be seen from the graph, there is a good match between the deflection predicted by simulation and the deflection on the real part.

3D printing can therefore be used to create load bearing parts with tailored compliance as well as complex shapes.

The production of the three dimensional features of BLUE was the most time consuming aspect of the mechanical build. Many of these elements, for example, the crossbars, are not under tremendous load and could be more quickly produced using 3D printing.

The spring in the arch of the foot of BLUE was remade using SLS 3D printing. This is a part which is under considerable load, which must be capable of controlled elastic deformation, and which connects together the two sides of the chassis of the foot.

Various designs for the foot arch were evaluated. It was found that the design shown in Fig. 7(*a*) performed with a better spring characteristic and overall stress distribution.

Figure 7(*b*) shows FEA analysis used during the design of the new arch part. The width and thickness of the part decrease as it nears the shaft connection in order to equalize bending and keep stresses roughly even over the part. At either end of the part, flares with M6 holes allow for connection to the waterjet cut aluminum sides of the foot. These holes are printed slightly undersize, then drilled, and tapped.

Figure 7(*c*) shows the FEA simulated deflection for the designed arch versus measurements taken from loading one of the fabricated parts. In simulation, the arch displays a linear stiffness profile, reaching a deflection of around 20 mm under a load of 250 N. As can be seen from the figure, the real arch is not as stiff as predicted by simulation, exceeding 20 mm deflection under a load of 200 N. After this point, additional loading is carried by the metal parts of BLUE, rather than the arch itself, so there is no danger of the fabricated part breaking, even though it is softer than desired.

We observed some hysteresis during the unloading of this part, however, it did return to its original state. We would like to carry out further load testing of this part in a Universal Testing Machine. The nonlinearity of the deflection of the fabricated part under heavy loading suggests that empirical analysis should be undertaken when utilizing such 3D printed parts under large loads.

3D printing provides a very easy way to produce the three dimensional features of a robot which is primarily constructed from waterjet cut parts. Parts, such as sensor and electronics mounts, cable routing parts, etc., are the most obvious application of 3D printing when supplementing waterjet cutting, but as we have shown, load bearing components can also be produced.

3.5 Producing Hybrid Parts With FDM Printing. Fused deposition modeling is another 3D printing technology which prints in layers, but instead of laying down an even layer of powder for every layer, FDM techniques only place material where it is required—typically by extrusion. This means it is possible to introduce additional parts into a partly formed FDM part, before continuing the print.

Waterjet or laser cut parts are perfect for coupling with FDM printing, as they are typically a uniform thickness. We can therefore print a shell for a metal part, pause the printing, insert the metal part, and then resume printing. When printing resumes, we can print on top of the metal part, sealing it in and producing a hybrid, single piece part of plastic with encased metal. Alternatively, any sheet material suitable for waterjet or laser cutting may be used, such as acrylics.

Figures 1(*c*) and 8 show a rear foot part from BLUE, modified to be produced using this hybrid technique. The part was produced on an Ultimaker 2 printer, which is commercially available at relatively low cost. This printer can be instructed to pause the print at particular layer heights, and for this part it is paused twice, first for insertion of the first plate, and a second time for insertion of the metal crossbar and the second plate. It is necessary to coat the face of any inserted metal parts with adhesive, otherwise the plastic will not adhere correctly and the print will fail.

Our experiment shows that this is indeed a feasible construction method. In this new rear foot part, there are two metal plates and one metal crossbar, which have all been waterjet cut. The plastic shell holds the crossbar in place, further simplifying the manual finishing process by allowing the drilling and tapping of the crossbar in situ, without a jig or a mill.

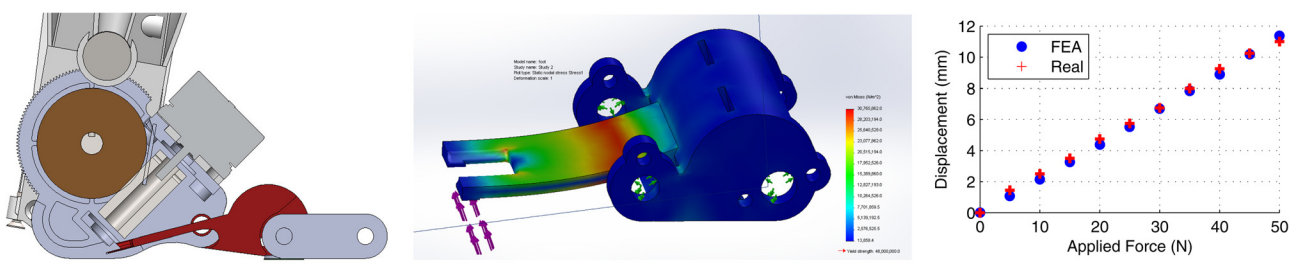

(a) (b) (c)

Fig. 6 Design and evaluation of the compliant feet of miniBLUE: (*a*) miniBLUE's foot, (*b*) FEA of miniBLUE foot arch, and (*c*) simulated and measured deflection of the arch

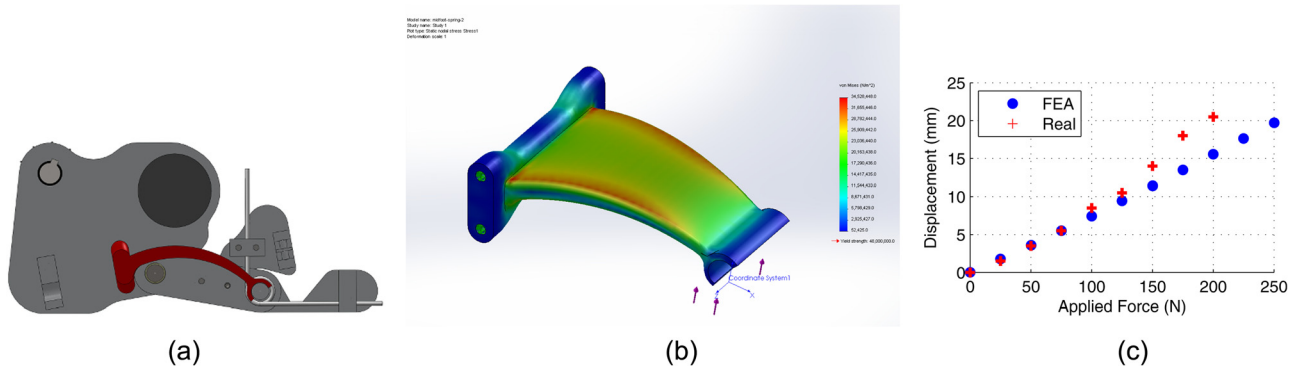

Fig. 7 Design and evaluation of the 3D printed compliant arch in the foot of BLUE: (*a*) BLUE's foot with 3D printed arch, (*b*) FEA of BLUE foot arch, and (*c*) simulated and measured deflection of the arch

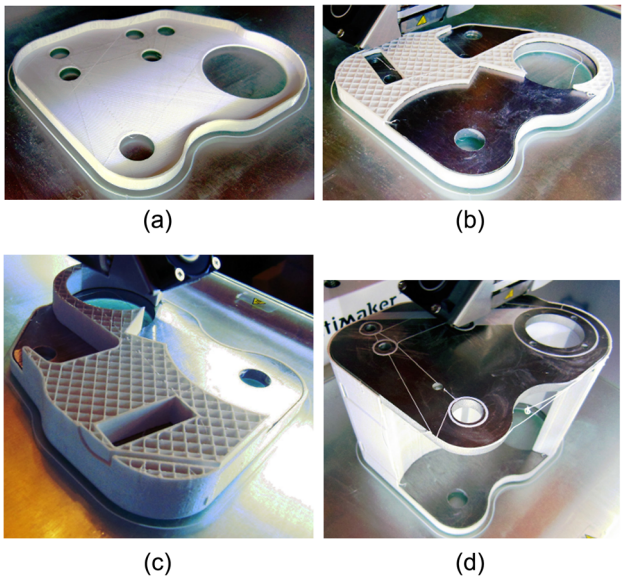

Fig. 8 FDM printing of hybrid part, encasing waterjet cut aluminum: (*a*) before first metal piece, (*b*) after first metal piece, (*c*) channel for sensor and recess for crossbar, and (*d*) all metal pieces in place

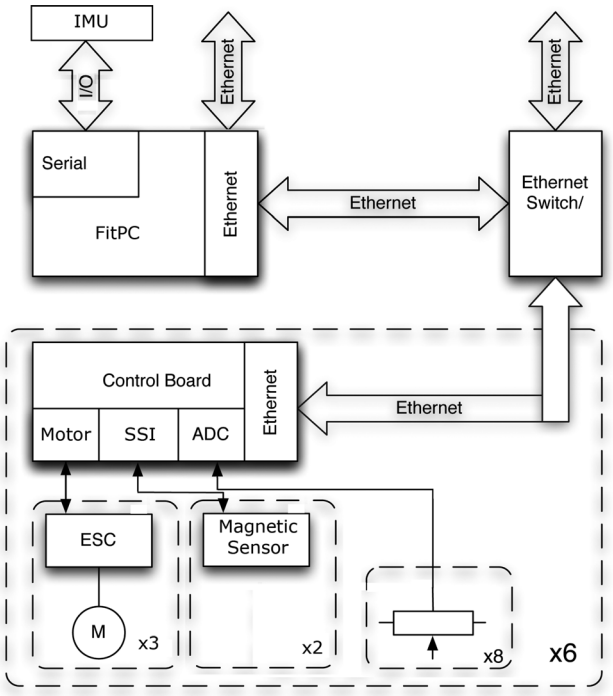

Fig. 9 The electronics layout of BLUE. Modular control boards linked via Ethernet network.

This hybrid technique produces a composite part which is strong and has three dimensional features and is a technique which can be utilized by labs with limited resources. It is a simple matter to integrate sensor mounts and cable routes, as is shown in the new rear foot for BLUE in Fig. 8(*c*). We will be producing more parts in this fashion and using them to produce replacement feet for BLUE, incorporating load sensors and padding to replicate the foot heel pad.

3.6 Design Lessons. We have shown that commonly available low-cost rapid manufacturing techniques such as waterjet cutting and 3D printing can be utilized to produce robots with complex joint structures, such as those in the variable impedance bipeds BLUE and miniBLUE. In particular, we have shown that SLS 3D printing can be used to create structural components with a tailored compliance, and how this can have a particular application in robots which must deal with contact forces.

We have also detailed a design for a robot which allows different types of variable stiffness mechanism to be tested more easily, retaining the structure, drive components, sensors, and electronics of the robot and allowing the variable stiffness mechanism to be removed and replaced in isolation. Given the continued work in the field of variable impedance mechanism design, it is very useful to have such a platform, which allows such mechanisms to be evaluated under similar conditions.

We have also introduced a hybrid manufacturing technique for producing plastic parts which have encased metal. This can be used for reducing the number of connecting elements required, allowing the streamlining of part geometry and reducing the risk of such connecting elements failing. We are currently using this technique to produce updated feet for BLUE.

4 Control and Validation

For both BLUE and miniBLUE, we have produced a distributed, modular electronics design based around an onboard Ethernet network. Ethernet has a very high bandwidth, allowing all joints to be commanded and all sensors read at a rate faster than 1 kHz, is relatively robust to noise, and is a multimaster protocol. We implement a custom protocol above the data link layer level. It is possible for the electronics of one joint to signal to the electronics of another joint, without involving the controlling PC. This is useful in the event that a failsafe is breached, in which case a signal can be sent to power down the whole robot, without

having to rely on the controlling PC. This functionality could also be used to implement local reflexive loops, similar to those seen in humans.

Figure 9 shows the control system architecture for BLUE. This is designed to be modular, with a control board based around an ATMEL microcontroller (AT91SAM7x) for each joint. Each of these control boards interfaces with up to three motor drivers to control the equilibrium position, stiffness setting, and damping of the joint. Each joint has two 10-bit magnetic position sensors (Austria Microsystems AS5040-ASSU, Unterpremstaetten, Austria), one for measuring the output position and one for measuring the deflection from equilibrium. These angle sensors are read through a digital synchronous serial interface (SSI) interface to reduce noise, which is typically only 0.3 deg. The current from the drive motors is also sensed. All sensors are read and the control loop run at a rate of 1 kHz, and digital filtering is applied to the sensor readings in order to reduce noise. Failsafe checks running on each board stop the robot if certain safe limits are reached, for example, if the average current passes a safe level.

For our robots, the failsafe checks include motor current and joint output position. The output position is a combination of the directly driven intermediate arm angle and the compliant deflection, our control boards calculate this actual output position and, for example, would allow the intermediate arm angle to exceed a safe joint output position, if the joint was appropriately deflected. This is necessary to make full use of the available compliance, while retaining protection against harm for the device.

The electronics of miniBLUE are similar to those of BLUE, with a set of control boards with ATMEL microcontrollers connected together through an on board Ethernet network. In contrast to BLUE, each control board on miniBLUE controls two joints and must therefore control up to six motors (two for position, two for stiffness, and two for damping). Maxon ESC boards (DEC50/5 with custom breakout board) are used by the control boards to drive the sensored EC motors which are used for position and stiffness.

4.1 Simulation. To validate that our hardware design should be capable of producing locomotion, with torques not exceeding the design limits of the device, we utilize full-physics simulations. Initially, we use joint trajectories gathered from human walking data.

We postulate that in addition to allowing the foot to better cope with uneven terrain, a compliant arch should reduce the shock loading that the foot is subject to. BLUE was simulated with three force sensors per foot, measuring the ground reaction forces on the heel, ball and toes of each foot. Each foot comprises three parts, and we varied the stiffness of the arch of the foot. For each stiffness value, we performed ten simulation runs and averaged the peak forces from the third step of each run. Figure 10 shows the peak forces measured by the force sensors on the toes, for three different walking gaits. A compliant foot arch leads to a reduction in shock loading on the foot. However, the arch of the foot must bear a significant load and so cannot be made too soft.

Trajectories are simulated before being run on the actual hardware, for example, as shown in Fig. 11. Our simulations predict that it should be possible to produce locomotive behavior within the design limits of the joints. However, dynamic simulations have many sources of errors, especially where impacts occur. To obtain a comparison between the simulation and the hardware, we produce a squatting motion on BLUE and change the joint stiffness during this motion.

This motion is shown for the knee joint of the robot simulated in Choreonoid in Fig. 12(*a*) and on the actual hardware in Fig. 12(*b*). The upper graph shows the sinusoidal trajectory of the intermediate arm, and that as the stiffness is reduced, the deflection under loading increases, and hence the joint angle deviates further from the intermediate arm angle. This deflection is shown in the lower graph, and we have found that the deflection matches that from our simulations, except for some additional backlash present on the hardware.

4.2 Initial Walking Experiments. To test the effects of different stiffness levels on walking behavior, we produced walking behavior on BLUE at different speeds and different stiffness levels. For this initial evaluation, the walking trajectory utilized was gathered from human data. V-REP [29] was used to dynamically simulate the robot performing walking motions from several minutes of continuous walking data. The performance of the robot was evaluated using a moving window cost function which rewarded judder-free forward motion and penalized torque. The walking data were segmented into areas which produced good walking behavior in the simulation, and individual steps were extracted from these segments. For the following experiments, a single trajectory is utilized and executed at different speeds and stiffness levels.

Naively commanding the robot to follow a given trajectory is unlikely to produce the desired result, especially when stiffness

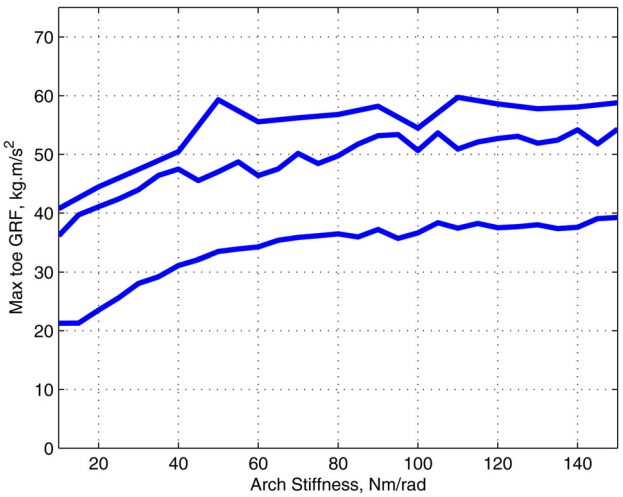

Fig. 10 Peak ground reaction forces (GFR) on the phalanges of the foot versus longitudinal arch stiffness, for three different walking gaits. Generally, a softer arch reduces peak GRF on the toes.

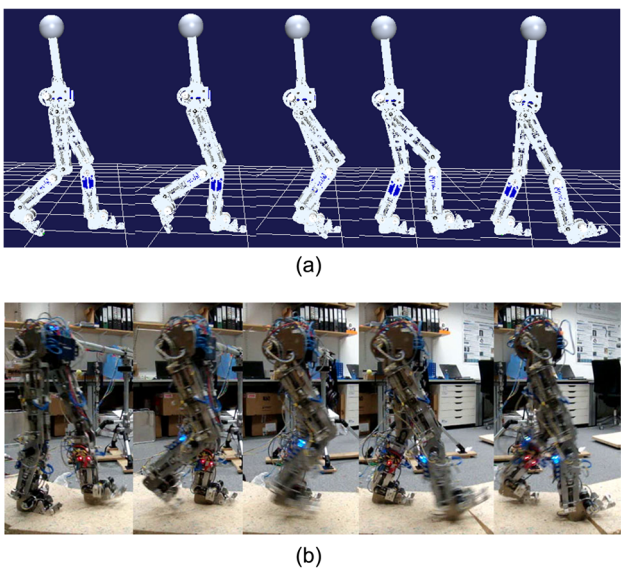

Fig. 11 Walking trajectory playback on the robot, both in simulation and on the actual hardware. (*a*) Simulation and (*b*) BLUE.

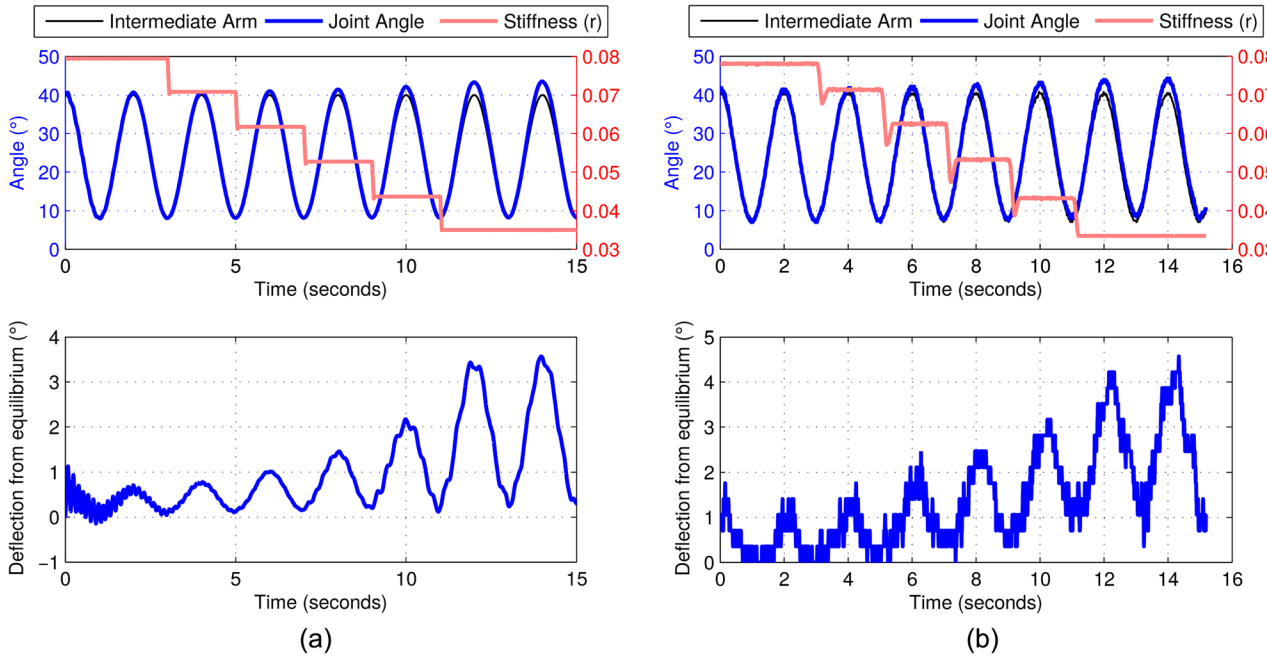

Fig. 12 Joint angles, equilibrium angles, stiffness setting, and deflection from equilibrium in the knee joint of BLUE during squatting: (*a*) simulation of squatting while changing stiffness and (*b*) hardware squatting while changing stiffness

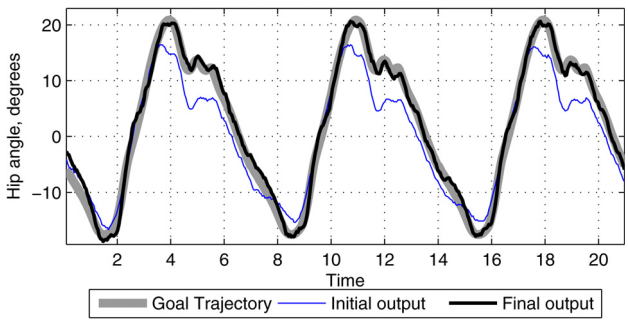

Fig. 13 Tuning the behavior of the robot to conform more closely to a desired output trajectory. Over three iterations, the output of the robot is pushed toward the desired result with a proportional gain.

levels are reduced and there is a lot of freedom for the joints to elastically deform. We therefore implemented a proportional gain trajectory iterator, which measured the final output position of the joints (intermediate arm position + elastic deflection) and attempted to compensate for deviations from the desired trajectory. An example of this process is shown for one of the hip joints of the robot, at slow speed and 40% stiffness, in Fig. 13. This figure shows a relatively good performance, the algorithm does not always match the desired trajectory so closely, and the following graphs show the deviation of the robot from this trajectory for each stiffness level.

Figures 14(*a*) and 14(*b*) show the performance of the robot walking at a slow speed and a faster speed, respectively, trying to reproduce the same trajectory at different stiffness levels. At each point on a trajectory, the digitally filtered current from each joint motor driver was sampled from that joint's controller board, and the current levels from all joints were integrated across each

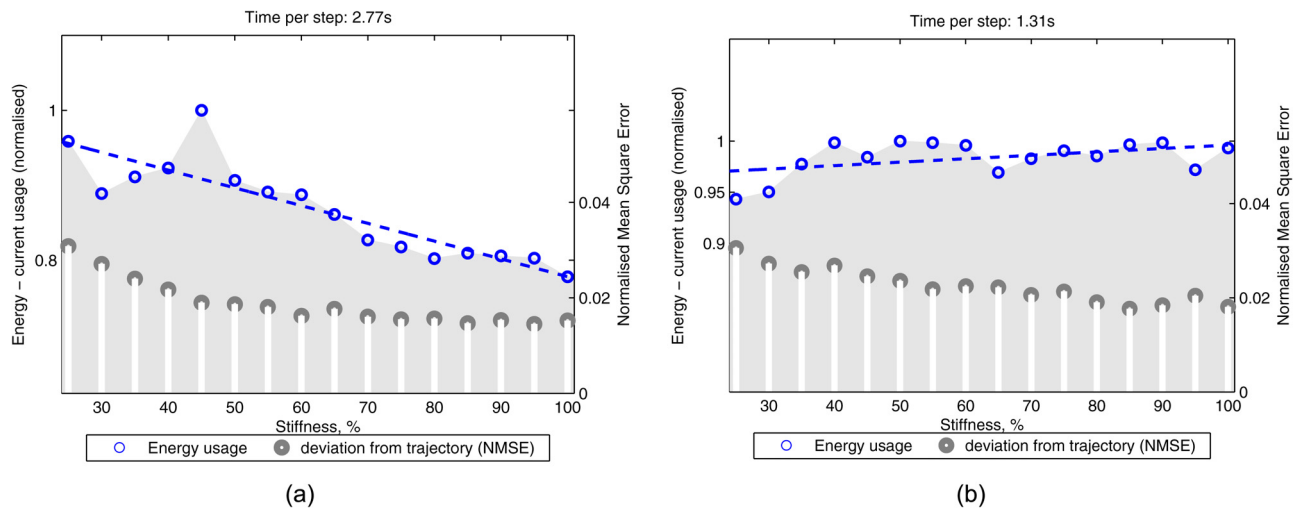

Fig. 14 Walking at a different stiffness levels, for two different speeds. (*a*) At very slow speeds, the task effectively becomes point-to-point motion, and we observe a higher energy usage in the robot at lower stiffness levels. (*b*) At faster speeds, decreasing the stiffness level can decrease energy usage.

trajectory run to produce a final value which represents a linear scaling of the electrical energy usage of the robot for that trajectory at that speed and stiffness level. For both graphs, each data point was sampled three times and the results were averaged.

Figures 14(*a*) and 14(*b*) also show the deviation of the output trajectory from the desired trajectory, as a normalized mean square error (shown on the right-hand axes). At lower stiffnesses, reproducing the exact trajectory is more difficult.

We observe from our results, at these speeds and others, that when running very slowly the current usage of the robot actually increases as stiffness decreases. We postulate that this is because the controller is effectively forced to "fight" the dynamics of the robot to try and keep to the desired trajectory. At quicker speeds, more close to the speed at which the trajectory was recorded, this effect is not seen. In fact, reducing stiffness reduced the current required to run the trajectory in some cases. This is beneficial not only because it reduced the energy consumption, but also because it makes the robot less susceptible to shocks and damage from disturbances when moving at these higher speeds.

So far, we have run the robot at relatively low speeds. We intend to run further experiments characterizing the behavior at faster speeds and also to explore whether there is an optimum stiffness level for a given walk at a given speed, at which energy efficiency and/or stability is maximized.

Our preliminary results point toward an advantage of having variable stiffness mechanisms, where behavioral flexibility is required. If slow, point-to-point motions are required, operation at a higher stiffness level may be better. For more dynamic locomotion, a lower stiffness level can be advantageous. This points toward benefits of variable impedance mechanisms in robots which are designed for more than locomotion at a particular speed.

5 Conclusion

Variable impedance technologies can play an important role in legged locomotion, but it is necessary to produce novel hardware in order to fully investigate this. We have detailed the construction of two such robots, BLUE and miniBLUE, both of which represent steps toward producing full three dimensional variable impedance bipeds.

An important aspect of our work is investigating how rapid manufacturing technologies can be used as enablers to allow the investigation of such hardware innovations. Typically, building a full bipedal robot from variable impedance joints is a costly and time consuming exercise, but by utilizing modern manufacturing methods, it is possible to make hardware more available to smaller laboratories and enable more design iterations at a faster pace. There have been a great deal of designs for individual variable impedance joints, but there has not been much exploration of these joints in larger systems. The manufacturing techniques shown here can make that possible, exemplified by miniBLUE, which allows the entire variable stiffness mechanism to be easily swapped.

We have shown that waterjet cutting and 3D printing can be used well in tandem to create complex robots, and that SLS 3D printing can be used to create structural compliant parts—for example, robot feet with compliant arches. Furthermore, we show a hybrid manufacturing process which fuses 3D printing and waterjet or laser cutting to produce strong parts with complex shapes, with a minimum of assembly and connective elements.

These rapid manufacturing techniques have been used to produce two uniquely capable bipedal robotic platforms suitable for the investigation of the effects of impedance modulation on bipedal locomotion. We have produced locomotive behavior at a variety of speeds and stiffness levels.

Our preliminary experiments suggest that varying the impedance of the robot joints has a measurable effect on the performance of the robot. We find that the best stiffness level for the robot joints may vary based on the conditions of the desired motions—for example, producing locomotion at various speeds, or more static movement tasks. This indicates that for a versatile bipedal robot, the use of variable impedance mechanisms can be advantageous over joints with a fixed level of stiffness.

Acknowledgment

This research was in part funded by the UKIERI, and in part by Grant Nos. EP/F500385/1 and BB/F529254/1 for the University of Edinburgh School of Informatics Doctoral Training Centre in Neuroinformatics and Computational Neuroscience[1] from the UK Engineering and Physical Sciences Research Council (EPSRC), UK Biotechnology and Biological Sciences Research Council (BBSRC), and the UK Medical Research Council (MRC).

References

[1] Collins, S., Ruina, A., Tedrake, R., and Wisse, M., 2005, "Efficient Bipedal Robots Based on Passive-Dynamic Walkers," Science, **307**(5712), pp. 1082–1085.

[2] Pratt, J., 2000, "Exploiting Inherent Robustness and Natural Dynamics in the Control of Bipedal Walking Robots," Ph.D. thesis, Computer Science Department, Massachusetts Institute of Technology, Cambridge, MA.

[3] Braun, D., Petit, F., Huber, F., Haddadin, S., van der Smagt, P., Albu-Schaffer, A., and Vijayakumar, S., 2013, "Robots Driven by Compliant Actuators: Optimal Control Under Actuation Constraints," IEEE Trans. Rob., **29**(5), pp. 1085–1101.

[4] Howard, M., Braun, D., and Vijayakumar, S., 2013, "Transferring Human Impedance Behavior to Heterogeneous Variable Impedance Actuators," IEEE Trans. Rob., **29**(4), pp. 847–862.

[5] Braun, D., Howard, M., and Vijayakumar, S., 2012, "Optimal Variable Stiffness Control: Formulation and Application to Explosive Movement Tasks," Auton. Robots, **33**(3), pp. 237–253.

[6] Radulescu, A., Howard, M., Braun, D., and Vijayakumar, S., 2012, "Exploiting Variable Physical Damping in Rapid Movement Tasks," IEEE/ASME International Conference on Advanced Intelligent Mechatronics (AIM 2012), Kachsiung, Taiwan, July 11–14, pp. 141–148.

[7] Nakanishi, J., Radulescu, A., and Vijayakumar, S., 2013, "Spatio-Temporal Optimization of Multi-Phase Movements: Dealing With Contacts and Switching Dynamics," IEEE/RSJ International Conference on Intelligent Robots and Systems (IROS 2013), Tokyo, Nov. 3–7, pp. 5100–5107.

[8] Vanderborght, B., Albu-Schäffer, A., Bicchi, A., Burdet, E., Caldwell, D. G., Carloni, R., Catalano, M., Eiberger, O., Friedl, W., Ganesh, G., Garabini, G., Grebenstein, M., Grioli, G., Haddadin, S., Hoppner, H., Jafari, A., Laffranchi, M., Lefeber, D., Petit, F., Stramigioli, S., Tsagarakis, N., Van Damme, M., Van Ham, R., Visser, L. C., and Wolf, S., 2013, "Variable Impedance Actuators: A Review," Rob. Auton. Syst., **61**(12), pp. 1601–1614.

[9] Enoch, A., Sutas, A., Nakaoka, S., and Vijayakumar, S., 2012, "BLUE: A Bipedal Robot With Variable Stiffness and Damping," 12th IEEE-RAS International Conference on Humanoid Robots (Humanoids 2012), Osaka, Japan, Nov. 29–Dec. 1, pp. 487–494.

[10] Mitrovic, D., Klanke, S., Howard, M., and Vijayakumar, S., 2010, "Exploiting Sensorimotor Stochasticity for Learning Control of Variable Impedance Actuators," 10th IEEE-RAS International Conference on Humanoid Robots (Humanoids 2010), Nashville, TN, Dec. 6–8, pp. 536–541.

[11] Van Ham, R., Vanderborght, B., Van Damme, M., Verrelse, B., and Lefeber, D., 2007, "MACCEPA, the Mechanically Adjustable Compliance and Controllable Equilibrium Position Actuator: Design and Implementation in a Biped Robot," Rob. Auton. Syst., **55**(10), pp. 761–768.

[12] Jafari, A., Tsagarakis, N. G., Vanderborght, B., and Caldwell, D. G., 2010, "A Novel Actuator With Adjustable Stiffness (AwAS)," IEEE/RSJ International Conference on Intelligent Robots and Systems (IROS), Taipei, Taiwan, Oct. 18–22, pp. 4201–4206.

[13] Jafari, A., Tsagarakis, N. G., and Caldwell, D. G., 2011, "AwAS-II: A New Actuator With Adjustable Stiffness Based on the Novel Principle of Adaptable Pivot Point and Variable Lever Ratio," IEEE International Conference on Robotics and Automation (ICRA), Shanghai, May 9–13, pp. 4638–4643.

[14] Morita, T., and Sugano, S., 1995, "Design and Development of a New Robot Joint Using a Mechanical Impedance Adjuster," IEEE International Conference on Robotics and Automation (ICRA), Nagoya, Japan, May 21–27, pp. 2469–2475.

[15] Morita, T., and Sugano, S., 1995, "Development of One-DOF Robot Arm Equipped With Mechanical Impedance Adjuster," IEEE/RSJ International Conference on Intelligent Robots and Systems (IROS), Pittsburgh, PA, Aug. 5–9, pp. 407–412.

[16] Choi, J., Park, S., Lee, W., and Kang, S., 2008, "Design of a Robot Joint With Variable Stiffness," IEEE International Conference on Robotics and Automation (ICRA 2008), Pasadena, CA, May 19–23, pp. 1760–1765.

[17] Tsagarakis, N., Sardellitti, I., and Caldwell, D., 2011, "A New Variable Stiffness Actuator (Compact-VSA): Design and Modelling," IEEE/RSJ

[1] www.anc.ac.uk/dtc

International Conference on Intelligent Robots and Systems (IROS 2011), San Francisco, CA, Sept. 25–30, pp. 378–383.
[18] Wolf, S., and Hirzinger, G., 2008, "A New Variable Stiffness Design: Matching Requirements of the Next Robot Generation," IEEE International Conference on Robotics and Automation (IROS), San Francisco, CA, Sept. 25–30, pp. 1741–1746.
[19] Uemura, M., and Kawamura, S., 2010, "A New Mechanical Structure for Adjustable Stiffness Devices With Lightweight and Small Size," IEEE/RSJ International Conference on Intelligent Robots and Systems (IROS 2010), Taipei, Taiwan, Oct. 18–22, pp. 2364–2369.
[20] Choi, J., Hong, S., Lee, W., Kang, S., and Kim, M., 2011, "A Robot Joint With Variable Stiffness Using Leaf Springs," IEEE Trans. Rob., **27**(2), pp. 229–238.
[21] Petit, F., Chalon, M., Friedl, W., Grebenstein, M., Schaffer, A., and Hirzinger, G., 2010, "Bidirectional Antagonistic Variable Stiffness Actuation: Analysis, Design & Implementation," IEEE International Conference on Robotics and Automation (ICRA 2010), Anchorage, AK, May 3–7, pp. 4189–4196.
[22] Laurin-Kovitz, K., Colgate, J., and Carnes, S., 1991, "Design of Components for Programmable Passive Impedance," IEEE International Conference on Robotics and Automation (ICRA), Sacramento, CA, Apr. 9–11, pp. 1476–1481.
[23] Laffranchi, M., Tsagarakis, N. G., Caldwell, D. G., and Sheffield, W. B., 2010, "A Variable Physical Damping Actuator (VPDA) for Compliant Robotic Joints," IEEE International Conference on Robotics and Automation (ICRA), Anchorage, AK, May 3–7, pp. 1668–1674.
[24] Herr, H., and Wilkenfeld, A., 2003, "User-Adaptive Control of a Magnetorheological Prosthetic Knee," Ind. Robot, **30**(1), pp. 42–55.
[25] Umberger, B. R., and Martin, P. E., 2007, "Mechanical Power and Efficiency of Level Walking With Different Stride Rates," J. Exp. Biol., **210**(Pt 18), pp. 3255–3265.
[26] Ker, R., Bennett, M., Bibby, S., and Kester, R., 1987, "The Spring in the Arch of the Human Foot," Nature, **325**(6100), pp. 147–149.
[27] Gefen, A., 2003, "The In Vivo Elastic Properties of the Plantar Fascia During the Contact Phase of Walking," Foot Ankle Int., **24**(3), pp. 238–244.
[28] Kappel-Bargas, A., Woolf, R. D., Cornwall, M. W., and McPoil, T. G., 1998, "The Windlass Mechanism During Normal Walking and Passive First Metatarsophalangeal Joint Extension," Clin. Biomech. (Bristol, Avon), **13**(3), pp. 190–194.
[29] Coppelia Robotics, 2013, "V-rep," Coppelia Robotics GmbH, Zurich, Switzerland, http://coppeliarobotics.com/